Comparative Analysis of Sentinel-1 and PlanetScope Imagery for Flood Mapping of Evros River, Greece

Christos Theocharidis*[a], Athanasios V. Argyriou[a], Alexia Tsouni[b], Mariza Kaskara[b], Charalampos (Haris) Kontoes[b]

[a] ERATOSTHENES Centre of Excellence, Franklin Roosevelt 82, 3012 Limassol, Cyprus;

[b] National Observatory of Athens, Operational Unit BEYOND Centre for Earth Observation Research and Satellite Remote Sensing IAASARS/NOA, GR-152 36 Athens, Greece

ABSTRACT

The Evros region in Greece is prone to frequent floods, causing significant damage to infrastructure and communities. It is imperative to have an effective flood monitoring system in place to mitigate the risks associated with these natural disasters. Satellite remote sensing technology can provide vital information for monitoring and assessing the impact of such events. High-resolution satellite imagery and other remote sensing techniques can provide near real-time information on the floods' extent, severity, and dynamics, allowing for prompt and accurate responses of disaster management. This study integrated radar and optical imagery from Sentinel-1 and PlanetScope, respectively, to map the extent of a significant flood event along the Evros River from 12th of January to 01st of February 2021. Moreover, it exploits geomorphometric information through Digital Elevation Models (DEMs) to assess the flood risk zones. The region experienced the highest recorded rainfall in the last 50 years, making the event particularly noteworthy. More specifically, the Hellenic National Meteorological Service recorded an average monthly rainfall of 408 mm for January and 211 mm for the first ten days of February. The outcomes of this study highlight the benefits of interdisciplinary approaches and the synergy within optical and radar imagery, which can offer vital data to local authorities and stakeholders in decision making towards mitigation strategies and resilience in flood risk events.

Keywords: Sentinel-1, SAR, PlanetScope, Flood, Evros, Natural Hazard, Google Earth Engine, MNDWI

*christos.theocharidis@eratosthenes.org.cy; c.theocharidis@cut.ac.cy

1. INTRODUCTION

Climate change has made its presence felt, leading to changes in precipitation patterns[1], sea level rise[2,3], and more frequent and intense extreme weather events[4]. Extreme weather events can cause damage to infrastructure, disrupt economic activities (e.g., farming), and lead to loss of life and displacement of people.

Floods can be described as the most frequent and devasting natural disaster causing critical issues for society and the environment [5]. The increasing frequency and severity of floods pose a tremendous challenge for emergency responders and decision-makers. In this context, satellite remote sensing and various image processing techniques, such as machine learning are effective in flood mapping, monitoring, and fast delivering accurate information to support decision-making processes [6,7].

In recent years, a large number of studies have evaluated the performance of different remote sensing techniques and data sources for flood mapping like utilising Low[8] and Medium[9] resolution satellites, integration between them[10], UAV systems [11], Multi-Criteria Decision Analysis (MCDA)[12] Artificial Intelligence (AI) [13] and Convolution Neural Networks (CNN) [14] methods. Among them, Sentinel-1 Synthetic Aperture Radar (SAR) and PlanetScope[15] optical imagery have shown their potential in mapping flood events, gaining increasing attention due to their high spatial and temporal resolution and wide coverage. Additional studies have revealed Sentinel-1 and PlanetScope image's full ability making them valuable tools for flood monitoring and forecasting, providing accurate and up-to-date information on flood extent, severity and dynamics [16–19].

1.1 Study area

This study focuses on northern Greece, the Evros district and particularly the Evros River, covering a buffer zone of 10 km from the river to the Greek territory. Being one of the longest rivers in Greece, the Evros River has a length of approximately 306 km, originating from Bulgaria and flowing through Greece and Turkey before reaching the Aegean Sea. Evros region is consisting of a diverse range of landscapes and ecosystems, including wetlands, forests and agricultural areas that constitute the dominant land cover within the buffer used in this study (Figure 1). However, the Evros River basin is also prone to flooding, particularly during winter and spring, when heavy rainfall and snowmelt occurs.

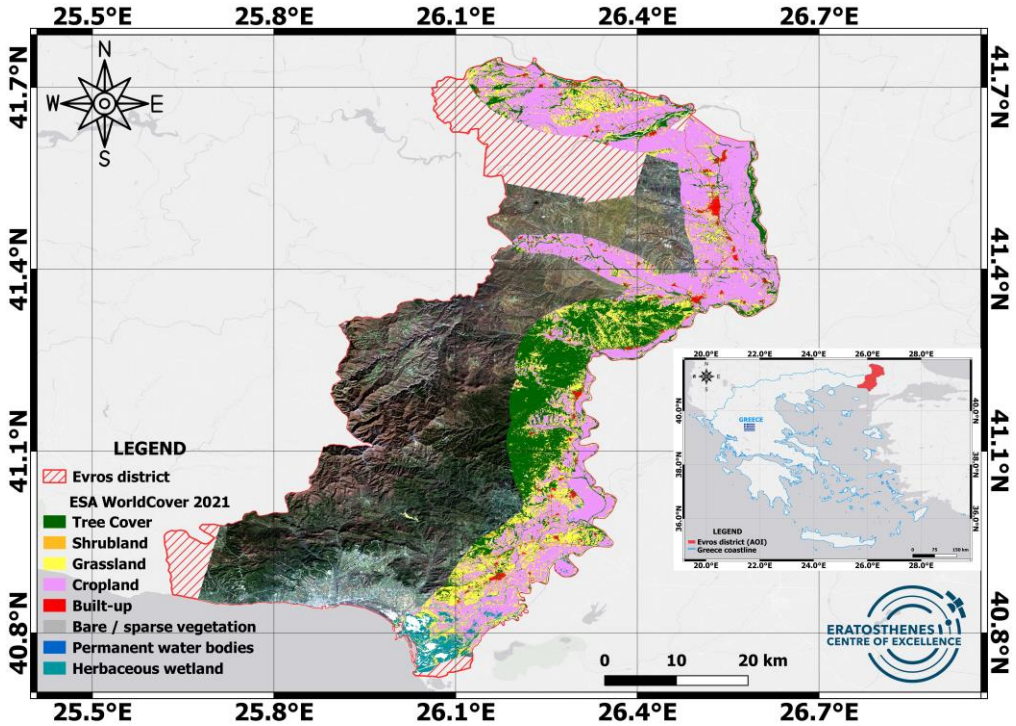

Figure 1. Area of Interest (Buffer zone 10 km) – Evros district with the ESA Landcover for 2021. The image is from PlanetScope from 15 January 2021 which did not cover the region of Evros at the given time.

1.2 Meteorological data

Between 12 January and 01 February 2021, due to unprecedented rainfall (a 50-year record), two major flooding events occurred, resulting in damage, mainly infrastructures and crops, leading a firefighter to death during a rescue operation [20] (Figure 2). Based on the Hellenic National Meteorology Service (EMY) stats, the monthly mean precipitation for January 2021 in the Evros district was 408 mm, where for the second 10-day period, the rainfall was 23 mm in Alexandroupolis, 50 mm in Ormenio (the northernmost village in Greece) and 86 mm in Soufli[21]. For February 2021, the rainfall ranged at 220 mm; particularly for the first 10-day period, the rainfall was 211 mm in Alexandroupolis and 81 mm in Soufli[22]. According to the Center for Hydrometeorology and Remote Sensing (CHRS), precipitation concentration maps were derived from 12th of January and 01st of February 2021, justifying the EMY rainfall measurements (Figure 3) spatially.

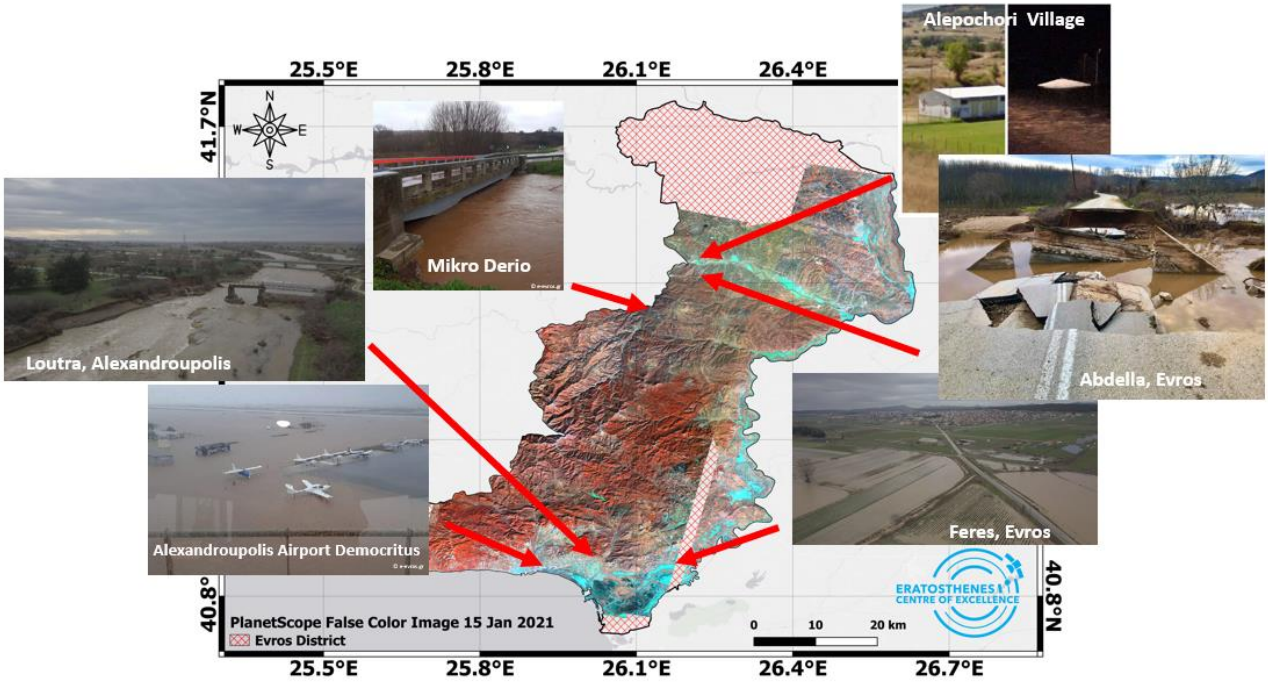

Figure 2. Examples of damage to infrastructure and crops caused by the flood in the Evros. Some photos sourced from e-evros.gr.

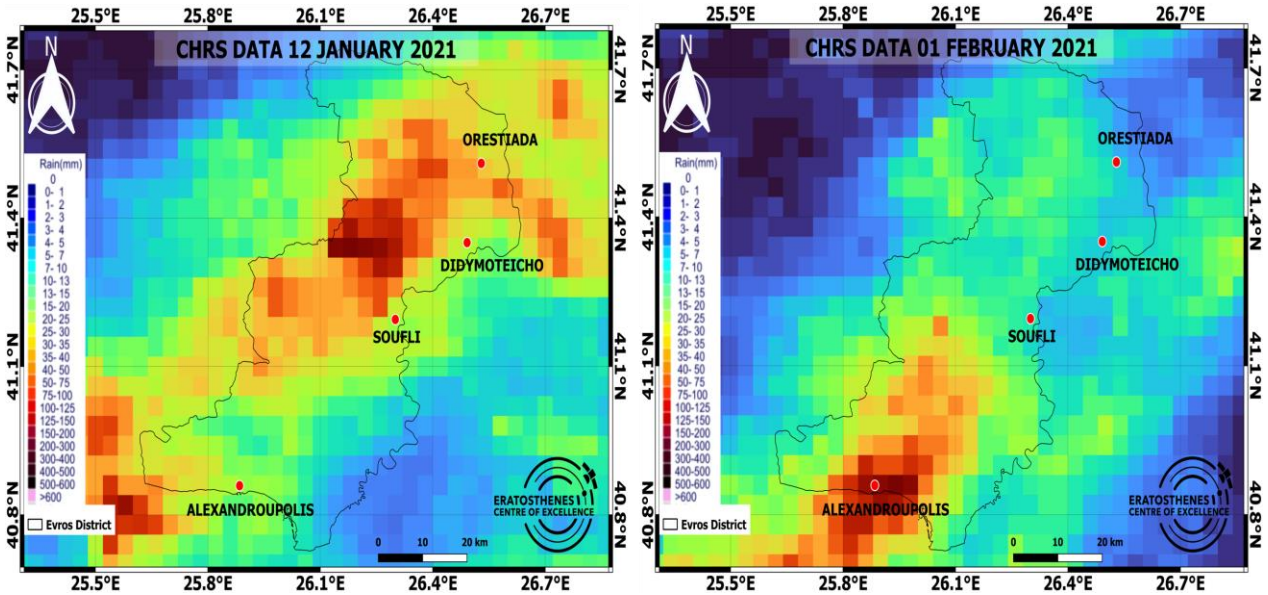

Figure 3. CHRS precipitation concentration data for the Evros district for 12 January 2021 (Left) and 01 February 2021 (Right).

2. METHODOLOGY

2.1 Workflow and datasets

This study used the workflow below (Figure 4), utilising Sentinel-1 and PlanetScope satellite data. Concerning the Sentinel-1 data, their pre-processing took place within Google Earth Engine (GEE) platform. Then the SAR Ground Range Detection (GRD) datasets (10m spatial resolution) were exploited to generate flood extent maps where a change detection approach was chosen to compare the before and after flood event images. The PlanetScope data (3m spatial resolution) were processed with the ArcGIS Pro software creating the Modified Normalised Difference Water Index (MNDWI) extracting the flood extent polygons. The MNDWI uses Green and SWIR bands for the enhancement of open water features. The formula of that index is given below in Equation 1. Furthermore, the Digital Elevation Model was utilised, generating from the System for Automated Geoscientific Analyses (SAGA) software the Topographic Wetness Index to retrieve the flood-prone areas. The TWI is a procedure for calculating the degree of wetness or dryness of the land is in a particular area, exploiting information about the steepness or the slope of the land derived from DEM, and showing how it interacts with water and flow accumulation to calculate the wetness. Generally, the TWI can expose areas likely to be flooded, for instance, after heavy rainfall, as in this study. After the creation of TWI and its classification based on natural breaks to highlight the higher risk zones in flooding, post-processing of Sentinel-1 and PlanetScope data was made to evaluate their performance and maps were generated by using the QGIS software.

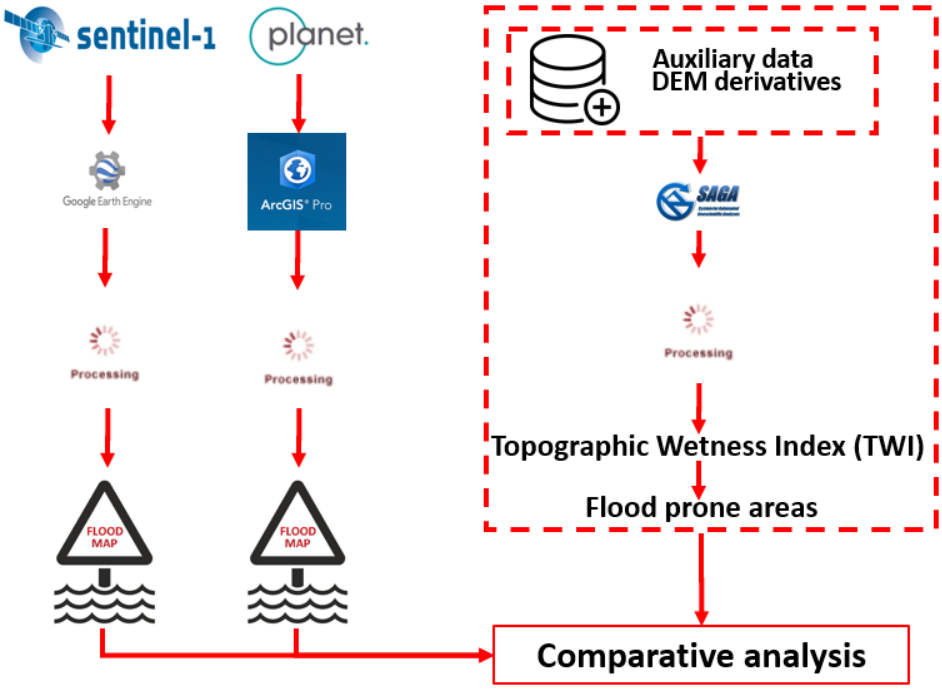

Figure 4. Flood mapping workflow used in this study.

As mentioned above, SAR (Sentinel-1) and optical imagery (PlanetScope) were used. More specifically for the Sentinel-1, images from 15th and 16th of January were used (3 and 4 days after the first flood event) since it did not cover the whole area with a single image, as indicated in Figure 5 with red dotted lines. Following the same logic, images from 02nd and 03rd of February were pre-processed (1 and 2 days after the second flood event). Concerning PlanetScope, it is clearly evident below that they did not cover the entire study area due to high cloud coverage, where for February, an image from 04th of February was used for the same reason. In addition, the ESA WorldCover at 10m spatial resolution was used as auxiliary data to extract the cropland, built-up and permanent water bodies areas. The first two areas were used to calculate how much of their area was affected by flooding, where the permanent water bodies were removed from the images to make more accurate estimations (Figure 6).

$$MDNWI = (Green - SWIR) / (Green + SWIR) \quad (1)$$

Where Green is the pixel values from the green band, and SWIR is the pixel values from the short-wave infrared band. In this case, instead of the SWIR band, the NIR band was used.

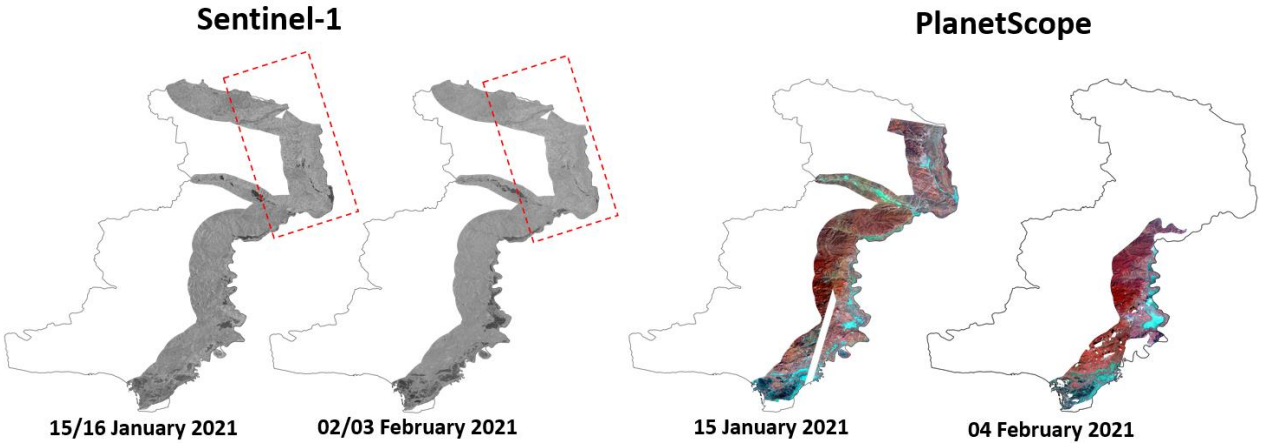

Figure 5. Left: Sentinel-1 GRD images. Right: PlanetScope false colour images.

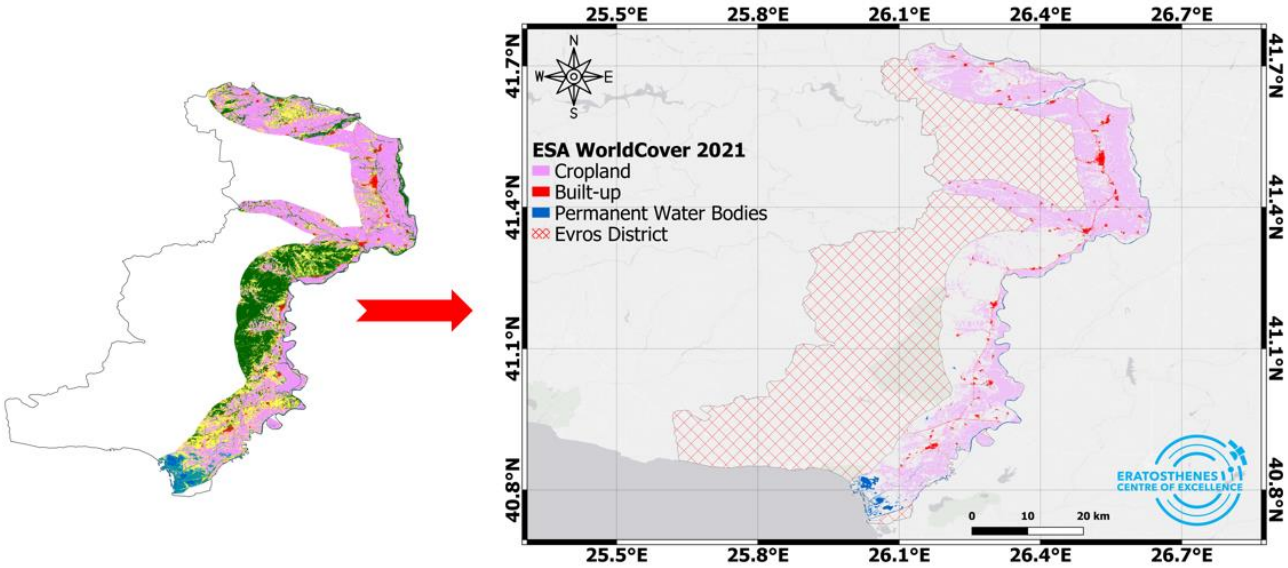

Figure 6. Left: ESA WorldCover 2021. Right: Cropland, Built-up and permanent water bodies as they extracted from the ESA WorldCover.

3. RESULTS

Comparing the Sentinel-1 images for January and February time frame, as it can be seen in Figure 7, a significant difference in the flood extent occurred. For the period of February, the estimated area is more than doubled compared to the January flood extent, assuming that the ground did not manage to drain the water in time. More particularly, the flood extent for January and February was estimated at 95.37 km^2 and 213.47 $km^{2,}$ respectively. Exploiting the Global Human Settlement Layer (GHSL) in GEE, the number of exposed people was estimated at 459 and 1155 people for January and February, respectively. The extracted data from the ESA WorldCover show that the affected cropland areas were estimated to be 86.48 km^2 and 186.91 km^2 for January and February, respectively, and the affected urban areas to 1.85 km^2 and 0.95 km^2.

Making a more thorough comparison, as indicated in Figure 8, the flood extent for 15th of January was estimated at 104.39 km^2 and 95.37 km^2 from PlanetScope and Sentinel-1, respectively. Assessing Case A in the map, image A1 indicates the flood extent as it was detected from Sentinel-1, where there were areas that the Sentinel-1 did not detect.

However, these gaps were filled by integrating the SAR data with the PlanetScope data, completing the flood mapping for that area at the given time. Another example is Case B, where PlanetScope did not detect a small area (B1 & B3 image) which Sentinel-1 did so (B2 & B4 image). It should be noted that the time of Sentinel-1 and PlanetScope image capture was with one day difference, so the later SAR image was captured more than 30 hours later. In the meantime, within this timeframe there was a rainfall event based on the CHRS data; thus, as shown in Case B (Figure 8) the SAR radar image, in comparison to PlanetScope one, is detecting an extra flooded extent coverage due to further rainfall. Additionally that may also happened since this specific area had a very high soil moisture rate detected by the radar image since the radar signal can be heavily affected by moisture[23].

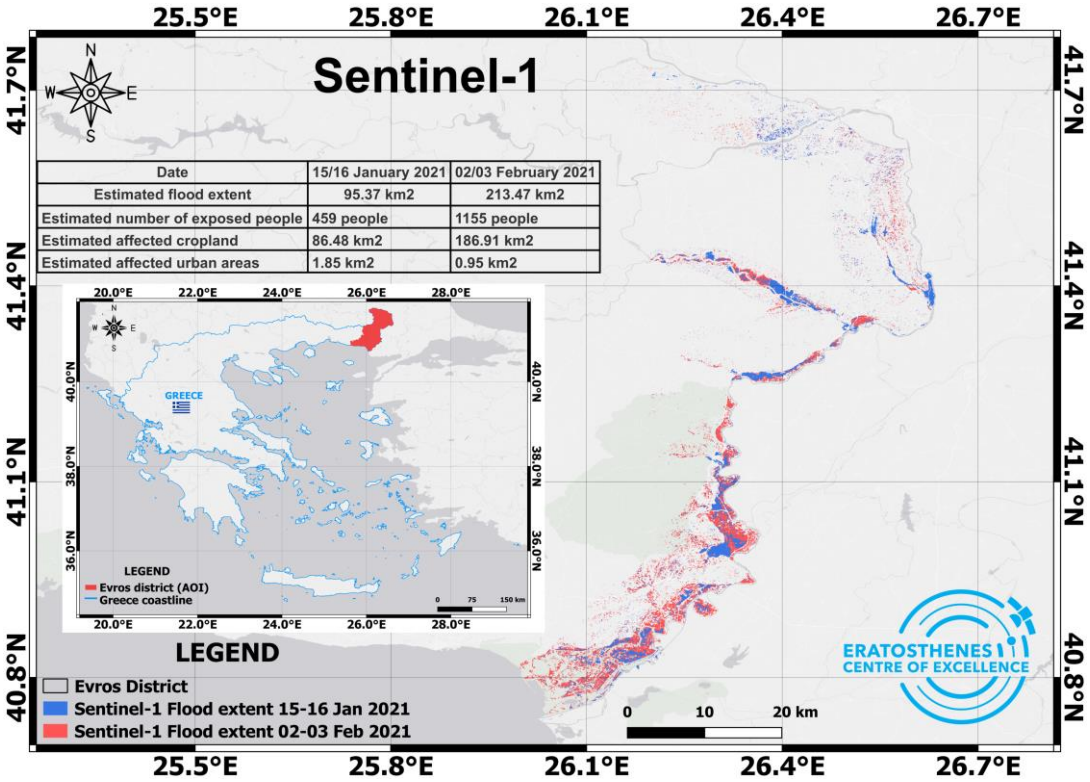

Figure 7. Comparison of the flood extents in the Evros region for January and February 2021 from Sentinel-1 images.

Following the same methodology, additional comparisons were made between the images of February, as indicated in Figure 9. However, they should not be taken into account since the images differ temporally (PlanetScope image is captured a day after the SAR images) and spatially (see Figure 5). Assessing Case A, it can be seen that PlanetScope did not properly detect the flooded crops (A1 image), where in the A2, A3 and A4 images, they can be observed as flooded from Sentinel-1. Continuing the analysis, in the area of Case A of Figure 9, the TWI revealed the flood-prone areas as shown in Figure 10A with blue colour. In Figure 10B and Figure 10C, SAR and optical flood data performed very well, overlapping the flood-prone areas from the TWI. Some possible reasons why the MNDWI did not detect the flooded crops properly could be the low reflectance, where crops may have low reflectance in the near-infrared band used to calculate the MDNWI, making it difficult to distinguish between water and not-water areas, mainly when crops are healthy and have high biomass. Another reason could be the MNDWI threshold used to classify the pixels as water or not. If the threshold is set too high, some flooded areas may not be detected, as in this case. Finally, another reason could be due to some limitations of the MNDWI since it may not be able to discriminate shallow from deep water bodies, making it sensitive to the presence of water but not to its depth. This can lead to false negatives if the water is shallow or other factors such as shadows or high vegetation cover are present.

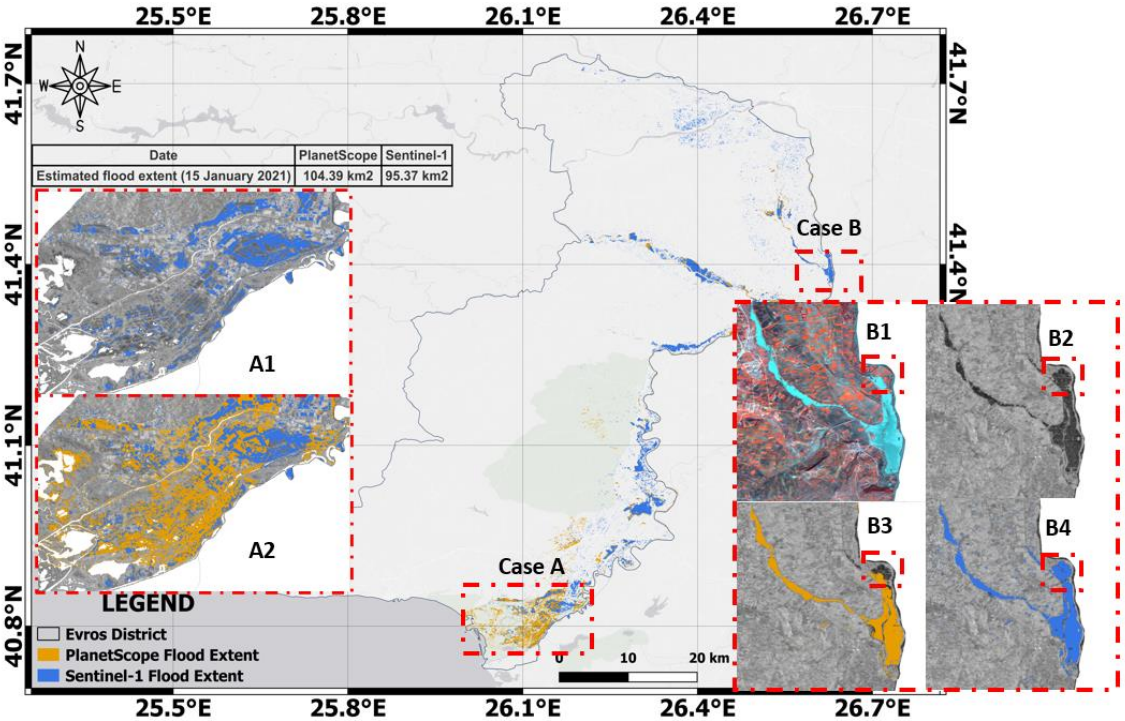

Figure 8. Comparison map between Sentinel-1 and PlanetScope flood extent on 15 January 2021.

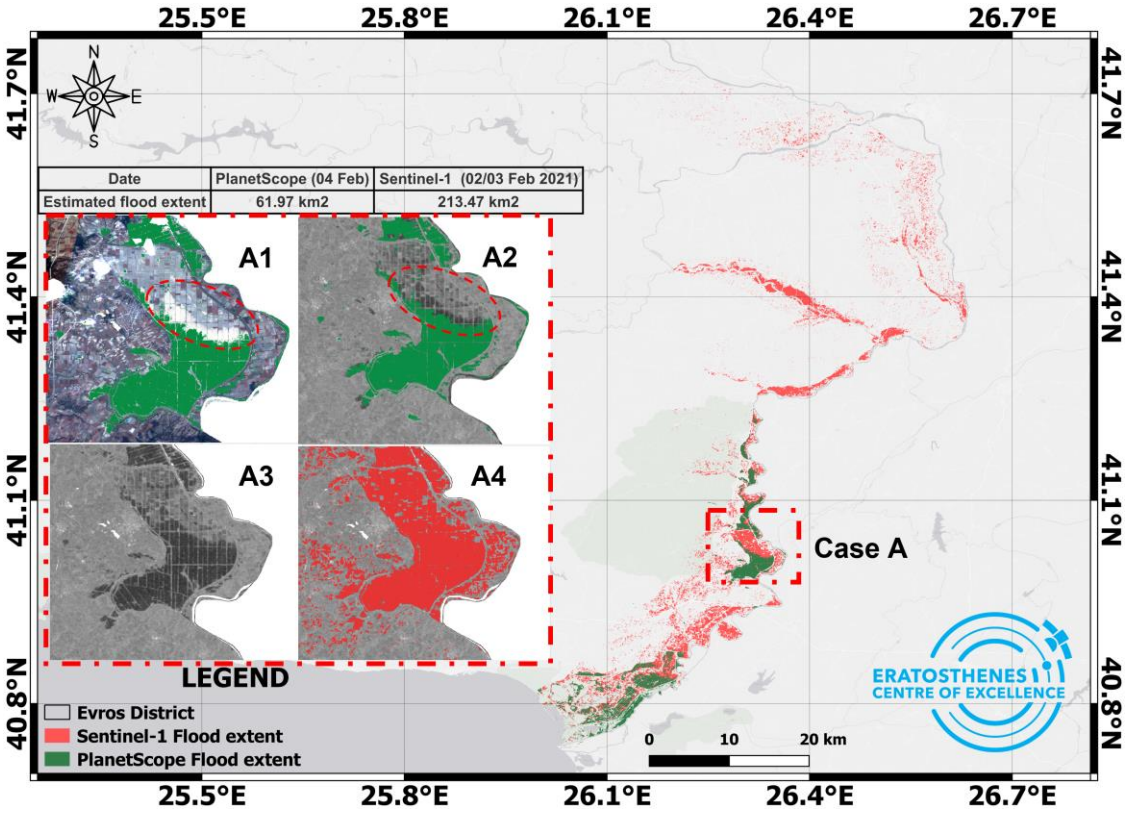

Figure 9. Comparison map between Sentinel-1 and PlanetScope flood extent on 02 to 04 February 2021.

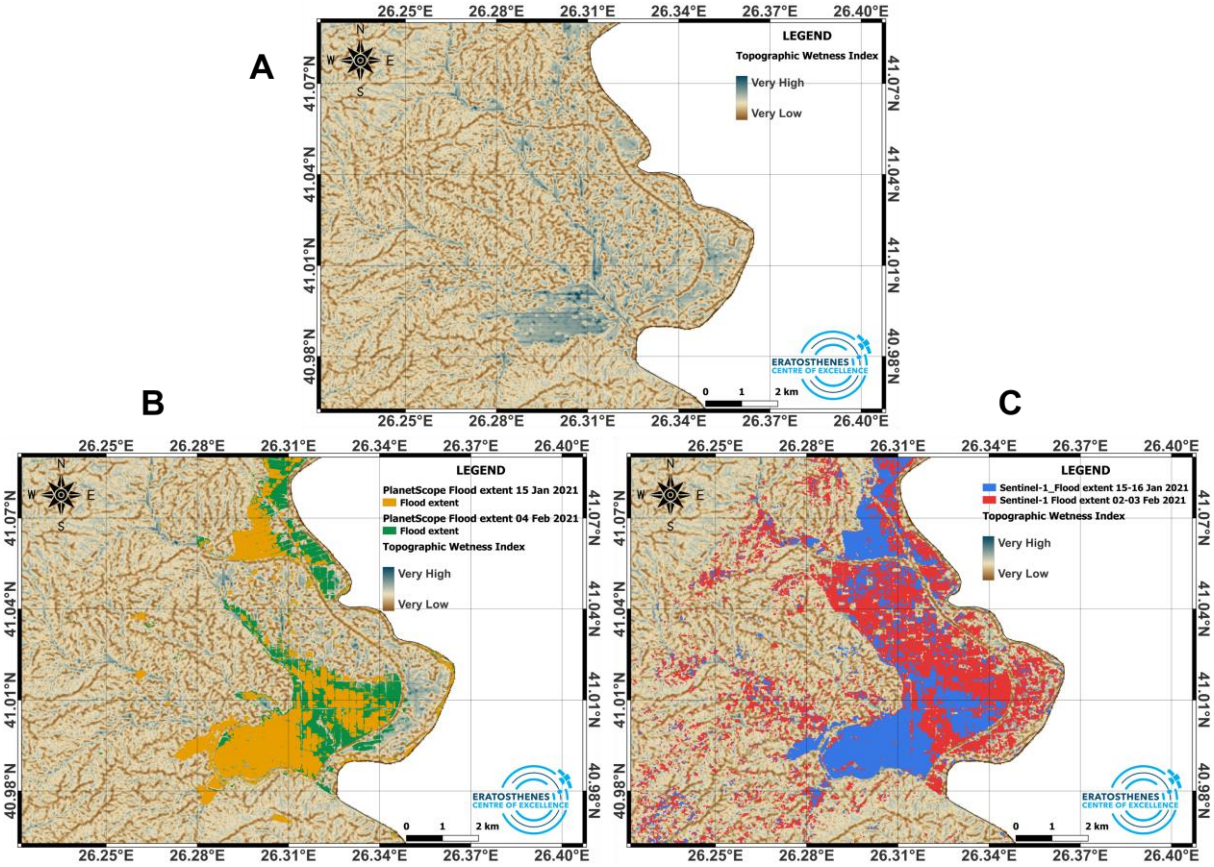

Figure 10. (A) TWI for Case A, as shown in Figure 9. High values indicate surfaces with higher moisture and alluvial deposits. Low values highlight areas with steep terrain and lower accumulation of moisture. (B) TWI with PlanetScope flood extent areas. (C) TWI with Sentinel-1 flood extent areas.

4. CONCLUSIONS

That comparative analysis provided useful outcomes about the performance of Sentinel-1 and PlanetScope data in mapping flood events. In some cases, SAR data performed better than PlanetScope despite its lower spatial resolution showing the full capabilities of SAR sensors to detect floods successfully. This study proved that combining the strengths of both remote sensing sensors can provide more accurate and reliable flood maps, since Sentinel-1 can penetrate clouds and deliver images of flood extents even in low light conditions, while PlanetScope data can provide higher spatial resolution images every day (depending on the location) taking advantage of it's frequent temporal coverage to spot flooded areas in more detail even in long term cloudy time frame periods in comparison to coarser optical sensors, such as Sentinel-2. Making a synergy of these two types of data can offer a more complete picture of the flood extent and its impacts on the surrounding area. Decision-makers can utilise this information to better understand the severity and extent of the flood, as well as to plan and allocate resources for emergency response and recovery efforts. By leveraging the benefits of both SAR and optical data, flood mapping can become a more powerful tool in mitigating the impacts of floods and protecting the safety and well-being of affected communities.
The script in GEE can be found at https://code.earthengine.google.com/6d6c1b0b8cd3e751df12d8312becb1a7

REFERENCES

[1] Ohba, M. and Sugimoto, S., "Differences in climate change impacts between weather patterns: possible effects on spatial heterogeneous changes in future extreme rainfall," Clim. Dyn. **52**(7–8), 4177–4191 (2019).

[2] Bernstein, A., Gustafson, M. T. and Lewis, R., "Disaster on the horizon: The price effect of sea level rise," J. financ. econ. **134**(2), 253–272 (2019).

[3] Schuerch, M., Spencer, T., Temmerman, S., Kirwan, M. L., Wolff, C., Lincke, D., McOwen, C. J., Pickering, M. D., Reef, R. and Vafeidis, A. T., "Future response of global coastal wetlands to sea-level rise," Nature **561**(7722), 231–234 (2018).

[4] Chen, Y., Moufouma-Okia, W., Masson-Delmotte, V., Zhai, P. and Pirani, A., "Recent progress and emerging topics on weather and climate extremes since the fifth assessment report of the intergovernmental panel on climate change," Annu. Rev. Environ. Resour. **43**, 35–59 (2018).

[5] Cornwall, W., "Europe's deadly floods leave scientists stunned" (2021).

[6] Farhadi, H., Esmaeily, A. and Najafzadeh, M., "Flood monitoring by integration of Remote Sensing technique and Multi-Criteria Decision Making method," Comput. Geosci. **160**, 105045 (2022).

[7] Uddin, K., Gurung, D. R., Giriraj, A. and Shrestha, B., "Application of remote sensing and GIS for flood hazard management: a case study from Sindh Province, Pakistan," Am. J. Geogr. Inf. Syst. **2**(1), 1–5 (2013).

[8] Minh, V. Q. and Huong, H. T. T., "Delineation of surface water using MODIS satellite image for flood forecast in the Mekong River basin," Int. J. River Basin Manag., 1–7 (2022).

[9] Farhadi, H. and Najafzadeh, M., "Flood Risk Mapping by Remote Sensing Data and Random Forest Technique," Water **13**(21), 3115 (2021).

[10] Zhang, F., Zhu, X. and Liu, D., "Blending MODIS and Landsat images for urban flood mapping," Int. J. Remote Sens. **35**(9), 3237–3253 (2014).

[11] Feng, Q., Liu, J. and Gong, J., "Urban Flood Mapping Based on Unmanned Aerial Vehicle Remote Sensing and Random Forest Classifier—A Case of Yuyao, China," Water **7**(12), 1437–1455 (2015).

[12] Gudiyangada Nachappa, T., Tavakkoli Piralilou, S., Gholamnia, K., Ghorbanzadeh, O., Rahmati, O. and Blaschke, T., "Flood susceptibility mapping with machine learning, multi-criteria decision analysis and ensemble using Dempster Shafer Theory," J. Hydrol. **590**, 125275 (2020).

[13] Syifa, M., Park, S. J., Achmad, A. R., Lee, C.-W. and Eom, J., "Flood Mapping Using Remote Sensing Imagery and Artificial Intelligence Techniques: A Case Study in Brumadinho, Brazil," J. Coast. Res. **90**(sp1), 197 (2019).

[14] Sarker, C., Mejias, L., Maire, F. and Woodley, A., "Flood Mapping with Convolutional Neural Networks Using Spatio-Contextual Pixel Information," Remote Sens. **11**(19), 2331 (2019).

[15] Planet Team., "Planet Application Program Interface: In Space for Life on Earth" (2017).

[16] Uddin, Matin and Meyer., "Operational Flood Mapping Using Multi-Temporal Sentinel-1 SAR Images: A Case Study from Bangladesh," Remote Sens. **11**(13), 1581 (2019).

[17] Avand, M. and Moradi, H., "Using machine learning models, remote sensing, and GIS to investigate the effects of changing climates and land uses on flood probability," J. Hydrol. **595**, 125663 (2021).

[18] Dong, Z., Wang, G., Amankwah, S. O. Y., Wei, X., Hu, Y. and Feng, A., "Monitoring the summer flooding in the Poyang Lake area of China in 2020 based on Sentinel-1 data and multiple convolutional neural networks," Int. J. Appl. Earth Obs. Geoinf. **102**, 102400 (2021).

[19] Li, C., Dash, J., Asamoah, M., Sheffield, J., Dzodzomenyo, M., Gebrechorkos, S. H., Anghileri, D. and Wright, J., "Increased flooded area and exposure in the White Volta river basin in Western Africa, identified from multi-source remote sensing data," Sci. Rep. **12**(1), 3701 (2022).

[20] Tasos Kokkinidis., "Firefighter Killed as Floods Hit Greece's Evros," 2021, <https://greekreporter.com/2021/02/01/firefighter-killed-as-floods-hit-greece-evros/> (9 April 2023).

[21] Hellenic National Meteorological Service., "Climatic Bulletin - January 2021," 2021, <http://www.emy.gr/emy/en/climatology/load_bulletin_html?fileid=366>.

[22] Hellenic National Meteorological Service., "Climatic Bulletin - February 2021," 2021, <http://www.emy.gr/emy/en/climatology/load_bulletin_html?fileid=368>.

[23] Le Morvan, A., Zribi, M., Baghdadi, N. and Chanzy, A., "Soil moisture profile effect on radar signal measurement," Sensors **8**(1), 256–270 (2008).

Acknowledgements
The authors acknowledge the 'EXCELSIOR': ERATOSTHENES: Excellence Research Centre for Earth Surveillance and Space-Based Monitoring of the Environment H2020 Widespread Teaming project (www.excelsior2020.eu). The 'EXCELSIOR' project has received funding from the European Union's Horizon 2020 research and innovation programme under Grant Agreement No 857510, from the Government of the Republic of Cyprus through the Directorate General for the European Programmes, Coordination and Development and the Cyprus University of Technology.